

HEAM : Hashed Embedding Acceleration using Processing-In-Memory

Youngsuk Kim, Hyuk-Jae Lee and Chae Eun Rhee

Abstract

In today’s data centers, personalized recommendation systems face challenges such as the need for large memory capacity and high bandwidth, especially when performing embedding operations. Previous approaches have relied on DIMM-based near-memory processing techniques or introduced 3D-stacked DRAM to address memory-bound issues and expand memory bandwidth. However, these solutions fall short when dealing with the expanding size of personalized recommendation systems. Recommendation models have grown to sizes exceeding tens of terabytes, making them challenging to run efficiently on traditional single-node inference servers. Although various algorithmic methods have been proposed to reduce embedding table capacity, they often result in increased memory access or inefficient utilization of memory resources.

This paper introduces HEAM, a heterogeneous memory architecture that integrates 3D-stacked DRAM with DIMM to accelerate recommendation systems in which compositional embedding is utilized—a technique aimed at reducing the size of embedding tables. The architecture is organized into a three-tier memory hierarchy consisting of conventional DIMM, 3D-stacked DRAM with a base die-level Processing-In-Memory (PIM), and a bank group-level PIM incorporating a Look-Up Table. This setup is specifically designed to accommodate the unique aspects of compositional embedding, such as temporal locality and embedding table capacity. This design effectively reduces bank access, improves access efficiency, and enhances overall throughput, resulting in 6.3× speedup and 58.9% energy savings compared to the baseline.

1 Introduction

Personalized recommendation serves as an important technology of various companies such as Meta [1], YouTube [2] and Netflix [3]. Recently, deep learning-based recommendation systems have emerged as a pivotal technology for improving the accuracy of predicting user-preferred content, thereby contributing to enhanced profitability for these companies. These advanced recommendation systems currently contribute substantially to the computational workload of the data center. Recent reports indicate that approximately 80% of data center resources are dedicated to the inference process of recommendation systems [4]. Recommendation models use dense features for user information and sparse features for item specifics through embedding operations. Following feature interactions, multi-layer perceptron (MLP)

layers generate click-through-rate (CTR) predictions, estimating the likelihood of user clicks on recommended items.

In large-scale data centers that extensively utilize embeddings, the embedding operation often becomes the primary factor influencing overall system performance. This stems mainly from the operation’s tendency to exhibit sparse and irregular memory access patterns. As a result, these memory-bound operations place significant constraints on traditional data center infrastructures [5], and this challenge continues to grow with the scale, as depicted in Figure 1. To tackle this challenge, recent efforts have concentrated on designing memory systems tailored to embedding operation [6], [7], [8], [9], [10], [11]. Approaches like TensorDIMM [6] and RecNMP [7] have explored the effectiveness of incorporating near-memory-processing (NMP) to alleviate the memory-bound nature by accelerating embedding operations directly within off-chip memory. These architectural solutions expedite the gather-and-reduce (GMR) process of embedding operations by deploying processing units in each rank of Dual Inline Memory Module (DIMM). This approach effectively harnesses the internal memory bandwidth, further amplified by the number of ranks in the memory channel. TRiM [8] and SPACE [9] followed a similar NMP structure while introducing other modifications to memory architecture. TRiM employed bank group-level processing-in-memory (PIM) within the DRAM device, while SPACE utilized High Bandwidth Memory (HBM) as a Dynamic Random Access Memory (DRAM) cache.

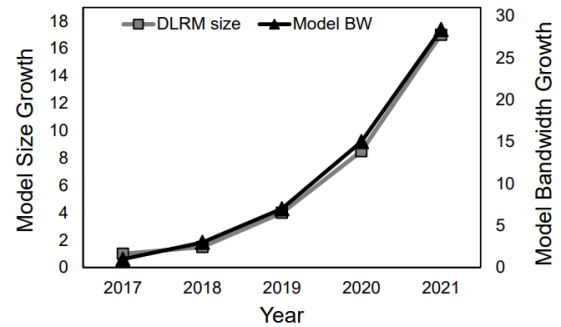


Figure 1. Model size and bandwidth growth of DLRM. (Reproduction from RecShard [12])

On the other hand, personalized recommendation models are currently expanding in size. According to RecShard [12], the memory capacity requirement of the Deep Learning Recommendation Model (DLRM) has been enlarged 16

times from 2017 to 2021, as shown in Figure 1. The model’s growth is attributed to the fact that more sparse features attribute to better model quality [12], [13]. However, The model operating on the inference server [5], [14], [15], [16] is significantly smaller in scale compared to the training model [12], [13]. Therefore, a significant gap exists between the training model size and the inference model size. Serving the inference with a multi-node server or introducing Solid-State-Drivers (SSDs) could be a possible solution. Still, it comes at the cost of synchronization and vulnerability to failures for the multi-node server case, and the SSDs have a negative impact on execution time [14], [17]. Therefore, exploring an alternative approach is essential to optimize model inference without encountering these drawbacks. Prior works took algorithmic approaches to reduce the embedding table size [18], [19], [20], [21]. While these techniques have successfully reduced the size of the embedding table, their work has been done at the cost of imposition of a much heavier burden on the memory bandwidth or inefficient memory capacity management. A representative method is compositional embedding [18], which employs a simple double-hashing technique to transform the original embedding table into a smaller quotient (Q) table and remainder (R) table. Nevertheless, this method necessitates double memory access, amplifying the memory-bound characteristics.

We propose HEAM, a specialized memory architecture integrated with PIM technology, designed to accelerate the inference process of compositional embedding. HEAM introduces a three-tiered memory hierarchy consisting of DIMM, HBM, and a lookup table (LUT). HBM is incorporated with base-die PIM (bd-PIM), while LUT serves as the storage space within bank-group PIM (bg-PIM), enhancing memory parallelism. The GnR processing in PIM can further reduce memory bandwidth requirements. This design is based on the following observations. Similar to original embedding, Q table exhibits high temporal locality characteristic within a small portion of entire embedding vector. Therefore, HEAM leverages HBM and DIMM to exploit this temporal locality. Notably, the R table, in particular, has a very small size and demonstrates a remarkably high temporal locality. Hence, we utilize an LUT within bg-PIM to store the entire R table. By addressing the memory bandwidth challenges associated with compositional embedding, HEAM effectively reduces the size of the embedding tables while simultaneously satisfying the requirements for memory bandwidth. This capability enables the execution of large models on a single-node server at a high processing speed. The primary contributions of our work can be summarized as follows:

- To the best of our knowledge, HEAM is the first work to address both the large model size problem and the memory-bound issue of the DLRM. HEAM successfully tackles both issues by designing specialized hardware for compositional embedding.

- We propose an allocation strategy for each hash table in compositional embedding. By distinguishing storage space for each table based on the analysis of their unique characteristics, HEAM achieves additional gains in bandwidth.
- We design a two-level PIM within HBM, specifically tailored for compositional embedding. This enables HEAM to expand into a three-tiered memory system, incorporating DIMM, HBM, and the LUT within PIM, thus effectively enhancing memory parallelism.

2 Background

2.1 Personalized Recommendation System

Recommendation System Overview. Among the various personalized recommendation models employed by diverse companies, DLRM stands out as one of the prominent recommendation system models. In the DLRM framework, inputs are categorized into two groups: dense features and sparse features. Dense features correspond to user information expressed as floating-point values, while sparse features facilitate access to items by transforming them into embedding vectors that encapsulate item-specific features. Figure 2 provides an illustration of the DLRM architecture. The bottom-mlp takes dense features as inputs, while the embedding lookup process handles sparse features. The embedding lookup operation gathers individual embedding vectors from multiple embedding tables, generating a single reduced vector. This reduced embedding vector is subsequently concatenated with the outcome of the bottom-mlp through a feature interaction layer. The resulting combined representation is then fed into the top-mlp. Once the top-mlp completes its calculations, the final outcome, CTR, is generated.

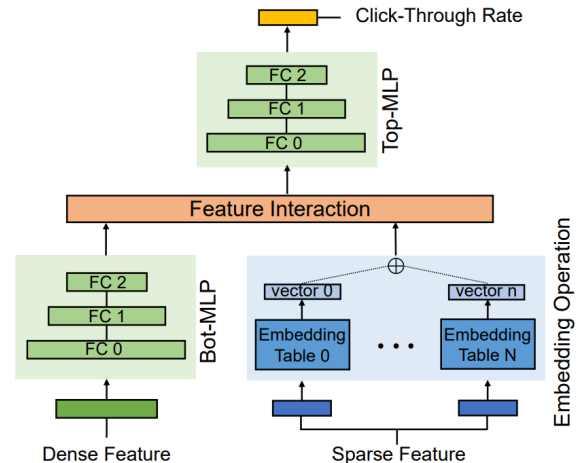


Figure 2. DLRM architecture

Challenges in Recommendation System Inference.

The performance of the recommendation system is constrained by the memory-bound nature of the embedding

operation. The irregular access patterns of embedding vectors, combined with the extensive size of the embedding table that surpasses the cache storage capacity on the host side, necessitate the frequent look-up of embedding vectors from the off-chip memory system. This frequent access to main memory leads to higher latency for the embedding operation than that of the bottom-mlp [9], classifying the model as memory-bound. Recently, recommendation models have been trending towards incorporating increasingly large-sized embedding tables, with their scale growing year by year [12]. Nowadays, industry-scale DLRM implementations require substantial memory resources, often reaching sizes of up to tens of terabytes, a significant portion of which is dedicated to housing embedding tables [14], [5]. Given that the quality of the model is closely linked to the size of these embedding tables, there is a strong incentive to utilize as large embedding tables as possible in production. However, the practical utilization of such large models is constrained by physical limitations, as the memory size of a single-node server is restricted by the available slots within the server.

2.2 Algorithms for Reducing Embedding Data Size

Algorithms Overview. Table 1 presents a comparison between aspects of algorithmic approaches for reducing embedding table size, including compression rates (Compression), accuracy relative to the original model (AUC), and operational characteristics such as bandwidth bound (BW bound) and memory friendliness (Mem. friendly). These methods could be categorized into three groups: Parameter Sharing (PS), Mixed Dimension (MD) and Generative Embeddings (GEN). The PS group utilizes hashing methods that map certain subsets of embedding vectors to the same vector. Conversely, MD group focuses on eliminating redundancy within the embedding dimensions, where embeddings that have minimal impact on the output are resized to a smaller dimension. Instead of storing embeddings as data, GEN group generates embedding from input indices using compute-intensive operations such as MLP. The PS group offers advantages regarding memory efficiency as its methods produce vectors with uniform dimensions as the algorithm’s output, promoting efficient utilization of memory capacity and accommodating memory system bursts effectively. Another benefit is the relatively low computational complexity of hash functions. However, the drawback is that the accuracy lags behind the baseline due to the semantic overlap among non-relevant embeddings. Furthermore, the degree of compression achieved is relatively modest. The MD and GEN groups attain a high compression rate and better model accuracy than the baseline. In the MD group, however, efficient use of memory resources is relatively hard since the output vectors vary in their dimension. Finally, the GEN group transforms the target model into the compute-bound application, which is far from the memory perspective, in contrast to other memory-bound groups. The MD and GEN

groups achieve a substantial compression rate while delivering improved model accuracy compared to the baseline. In the MD group, however, efficient utilization of memory resources is relatively challenging because the output vectors exhibit varying dimensions. On the other hand, the GEN group transforms the target model into a compute-bound application, diverging significantly from the memory-oriented perspective of the other groups, which are memory-bound applications.

Table 1. Comparison of embedding table reduction schemes.

Group	Method	Compression	AUC	BW bound	Mem. friendly
PS	Hashing [22]	Low	Much Lower	Memory	✓
	QR [18]	Moderate	Lower	Memory	✓
MD	MDE [19]	Moderate	Better	Memory	✗
	OptEmbed [21]	High	Better	Memory	✗
GEN	TT-Rec [20]	High	Better	Compute	✗
	DHE [23]	High	Better	Compute	✗

Compositional Embedding. Compositional embedding employs two types of hash functions, effectively partitioning the original embedding table into two smaller tables, as depicted in Figure 3 (a). These hash functions include the quotient operation and remainder operation. Embeddings that yield the same quotient result are mapped to corresponding vectors in the table generated by the quotient function (Q table). In contrast, embeddings with identical remainder results are directed to the same vector within the other hash table (R table). The total table size is typically reduced by a factor approximately equal to the inverse of the hash collision, with the R table size being usually negligible compared to that of the Q table. The R table size corresponds to the hash collision, whereas the Q table size is equivalent to the original table size divided by the hash collision. To process the embedding operation, it is necessary to reconstruct the original embedding. This is accomplished by performing straightforward mathematical operations on the vectors extracted from each table. The overall scheme is illustrated in Figure 3 (b).

2.3 NMP/PIM Designs for Recommendation System

Recent studies have introduced NMP units within the DRAM architecture to meet the memory bandwidth requirements of recommendation systems. Specifically, these approaches have incorporated multiple DIMMs with NMP units situated within their DIMM/Rank configurations, effectively exploiting DIMM/Rank-level parallelism [6], [7] to achieve increased throughput. TRiM [8] focused on the tree topological structure of the DRAM’s data path, further enhancing parallelism by integrating PIM units within each bank group. In pursuit of additional speedup, the aforementioned designs have leveraged the long-tail distribution of embeddings, where a small subset of embeddings is frequently reused. This has been accomplished by incorporating a cache

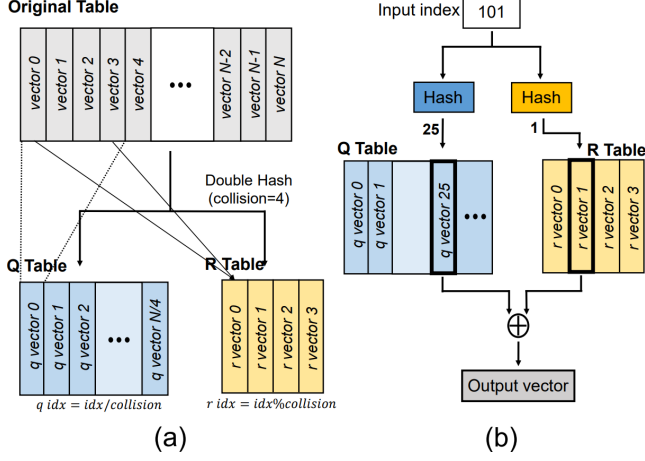


Figure 3. Compositional embedding overview. (a) Double hashing process (b) Embedding vector reconstruction process

within the buffer chip [7] or implementing load-balancing techniques with the assistance of the memory controller [8].

While it is possible to increase the throughput of the embedding operation by incorporating more DIMMs with NMP designs from previous approaches, this may lead to inefficiencies in power consumption [9]. To address this challenge, SPACE [9] introduced a heterogeneous memory system that combines HBM and DIMMs, with HBM functioning as a DRAM cache. Additionally, SPACE exploited the reduced locality of embedding vectors and the long-tail distribution of embedding vectors to achieve significantly higher throughput. In summary, achieving high performance in recommendation systems relies on core techniques that involve exploiting parallelism within the main memory and capitalizing on the long-tail distribution of embedding vectors.

3 Analysis on Compositional Embedding

As shown in Section 2.2, compositional embedding exhibits several advantages over other previously proposed schemes concerning the memory system. While alternative methods may yield better model prediction quality and higher compression rates, the nature of the output data poses challenges for the memory system when supporting the embedding operation. Consequently, we have selected compositional embedding as the target algorithm. In this section, we offer an in-depth analysis of the characteristics of compositional embedding.

3.1 Impact on DLRM Throughput

Compositional embedding further intensifies the memory-bound characteristics of the model by doubling the overall number of accesses to the main memory. This is because generating input vectors for the model necessitates accessing

two hash tables. Figure 4 (a) presents a comparison of the execution times for embedding operations on HBM and DIMM between the original model and the model with compositional embedding applied. The results indicate that compositional embedding leads to a 25% longer execution time on HBM and a 40% longer execution time on DIMM. Although the decrease in throughput is less pronounced on HBM due to its significantly higher number of channels compared to DIMM, it is evident that employing the compositional embedding results in increased memory access. This underlines the need for higher bandwidth than what traditional memory systems can provide.

3.2 Temporal and Spatial Locality

To investigate the locality characteristics in compositional embedding, we simulated cache behavior with embedding traces from criteo-kaggle-dataset [24]. A 4-way set associative cache is used during the experiment. Note that MLP weights are not included during the simulation, thereby producing a high cache hit rate of embeddings.

Temporal Locality. To find out the presence of temporal locality, we followed the method used in RecNMP [7]. We increased cache size from 1MB to 4MB and examined the difference in hit rate of random traces and traces generated from criteo dataset [24], [25] with compositional embedding applied, as depicted in Figure 4 (b). The total hit rate of compositional embedding is the summation of Q table and R table hit rate, which is much higher than that of the random traces. This result implies the temporal locality characteristics of double-hashed embeddings. Although hit rate of Q table is slightly smaller than R table, it is still much higher compared to random traces, indicating strong temporal locality of Q table embeddings which resembles to original table locality characteristics examined in prior works [7], [9]. This is due to the similar long-tail distribution between the original and the Q table, as illustrated in Figure 5. According to Figure 5 (a), a small subset of total embeddings takes the majority of the access. We refer to this subset as *hot vectors*. As the number of hot vectors is small, they are sparse across the embedding table. When quotient hashing maps consecutive embeddings to the same embedding, hot vectors tend to remain as hot vectors since the access rate of Q table embedding is identical to the access rate summation of consecutive embeddings that are mapped to that Q table embedding. Therefore, long-tail distribution remains as shown in Figure 5 (b).

As depicted in the Figure 4 (b), R table cache hit rate occupies fixed, high portion of the total hit rate across all the cache size. This indicates each vector inside R table presents high temporal locality. The main reason is the smaller size of R table compared to Q table, even though both tables are accessed concurrently to construct the input embedding. This concentrates R table access on a small number of embeddings, significantly increasing temporal locality. It is worth

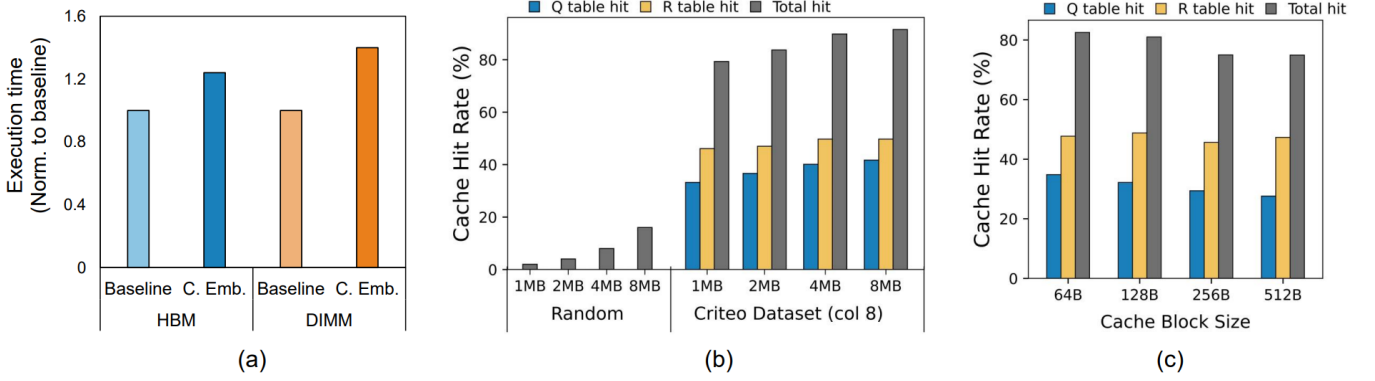


Figure 4. Compositional Embedding Analysis (a) Execution time comparison between original DLRM and compositional-embedding-applied DLRM (b) Verifying temporal locality by increasing cache size from 1MB to 4MB with vector length of 64B (c) Spatial locality by increasing cache line size from 64B to 512B where cache size is fixed to 1MB with vector length of 64B

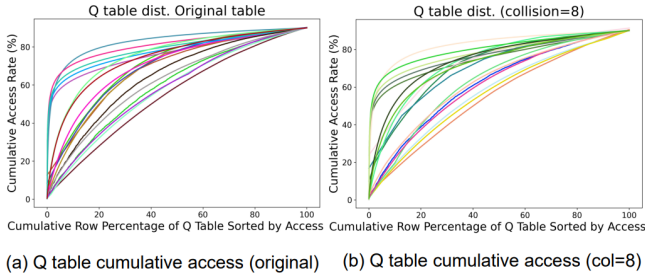


Figure 5. Cumulative access distribution of tables. (a) Original table (b) Q table with hash collision=8.

noting that R table embeddings display uniform distribution as illustrated in Figure 6, which is more intensified when hash collision is low as illustrated in the figure. Since the hot vectors are randomly widespread across the embedding table, the remainder hash function maps hot vectors randomly to the R table embeddings. Coupled with the fact that R table exhibits high temporal locality, uniform access distribution of R table embeddings indicates that all the R vectors are hot vectors.

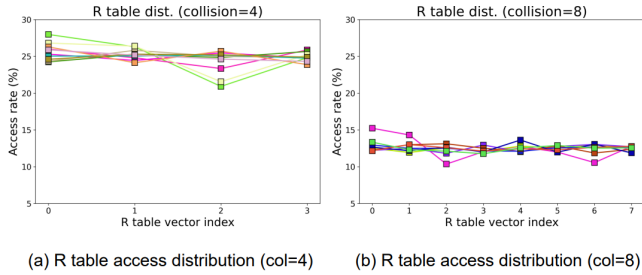


Figure 6. R table access distribution of 10 embedding tables. (a) Distribution with the collision of 4 (b) Distribution with the hash collision of 8. All embeddings have similar access distribution.

Spatial Locality. The simulation on spatial locality was conducted by measuring the hit rate of 64B length vector on 1MB cache, varying the cache line size from 64B to 512B on 1MB cache, again following the method used in [7]. Results are shown in Figure 4 (c). The observation shows that Q table cache hit rate decreases slightly, indicating little spatial locality. However, the R table cache hit rate implies that a mild spatial locality exists since the overall cache hit rate is stable, even though increasing cache line size diminishes the effect of temporal locality, suggesting the existence of spatial locality. Despite the presence of R table spatial locality, it is challenging to benefit from such characteristics as its impact is minimal. Furthermore, the embedding dimension exceeds traditional cache line size, as the vector length utilized in the recommendation system typically ranges from 64B to 512B. Fetching multiple R table vectors within a cache line is impossible, although R table vectors might be placed next to each other.

3.3 Opportunities for PIM Support

The above assessments suggest that enhanced throughput support is necessary for running compositional embedding during the inference stage. Inspired by the previous works that utilize NMP/PIM to extend the bandwidth [6], [7], [8], we conclude that employing PIM is an effective solution for addressing the memory-bound characteristic of compositional embedding. Two attributes of compositional embedding make the usage of PIM more effective. First, as described in Section 2.2, the data arrangement is suitable enough to employ the PIM architecture. This is due to the uniformity in vector dimensions, which ensures efficient use of memory capacity and consistency in the total DRAM burst needed for each vector. Second, unique features of the R table vectors, high temporal locality, and its uniform memory access distribution could be efficiently exploited by extending the PIM design to increase the throughput further. Integrated with a

heterogeneous system consisting of DIMM and HBM with base die PIM, the utilization of PIM is an effective design for supporting compositional embedding.

4 HEAM Architecture

4.1 Architecture Overview

We propose HEAM, a specialized memory system designed to enhance the bandwidth of DLRM when compositional embedding is employed. The overall architecture is depicted in Figure 7. As illustrated in Figure 7 (a), the HEAM system incorporates a heterogeneous memory architecture that comprises HBM and DIMM, which addresses the memory-bound nature to some extent by offloading frequently accessed vectors to HBM. Nonetheless, it’s important to note that the overall memory access demands double when employing compositional embedding. As a result, depending solely on HBM remains insufficient to achieve the required throughput.

To tackle this problem, we design a two-level PIM system within the HBM to enhance the throughput by utilizing in-memory parallelism, thereby providing additional bandwidth support for the embedding operation. In Figure 7 (b), the first-level processing unit is located on the base die of the HBM, whereas the second-level processing units are located inside each bank group. These processing units are referred to as bd-PIM and bg-PIM, named based on their respective locations. Within these PIMs, the embedding operation is processed in a two-stage partial addition fashion. Initially, each bg-PIM collects Q embeddings and their corresponding R embeddings from its dedicated bank group. Local addition is performed inside each bg-PIM on the collected embedding vectors, generating partial results. Once all bg-PIMs complete their respective operations, all the reduced vectors are forwarded to the bd-PIM. The same operation is carried out within the bd-PIM for each set of partial results, resulting in the final output delivered to the host processor.

Figure 8 (b) depicts the PIM architecture of bg-PIM. The system inside bg-PIM is equipped with an instruction register, an instruction decoder and a Multiply-and-Accumulate (MAC) unit. Additionally, LUT is integrated inside each bg-PIM to leverage the temporal locality of the R table described in Section 3.2. Therefore, the access to R embedding vectors is always directed to the LUT, decreasing the total bank access. HEAM employs batching of 4 embedding operations to address the load imbalance issue, following the technique utilized in RecNMP [7]. To avoid introducing too much area overhead into bank groups, we use up to 4 batch in our system. The bd-PIM receives partial sums delivered from bg-PIM and processes the final GnR operation as illustrated in Figure 8 (a). Note that the architecture of the bd-PIM is similar to that of the previous works.

4.2 Hash Table Allocation Strategy

To mitigate the double memory access problem associated with compositional embedding, we store the R and Q tables in memory in different ways. This is based on the data access patterns for each table are distinct and exhibit significant variation. Consequently, we ensure more efficient use of memory system resources. As these data access patterns are established after the training phase, we collect this distribution information prior to entering the inference stage. This additional process incurs minimal overhead, as demonstrated in previous studies such as [7] and [9].

Mapping Scheme for Q table. As the Q table typically exhibits a long-tail distribution similar to that of the original embedding table, we leverage an approach inspired by SPACE [9] to exploit the Q table’s characteristics. Embedding data with high temporal locality is offloaded to HBM, while the remaining embedding data are stored in DIMMs. The proportion of data to be offloaded to HBM is determined based on the bandwidth ratio between HBM and DIMM. This strategy, which involves gathering embedding data with high locality from HBM and fetching the rest from DIMMs, enhances the overall parallelism between the different memory types.

Mapping Scheme for R table. As described in Section 3.2, access to the R table is repeatedly conducted for a very limited set of data, consequently, all the data within the R table exhibits extremely high temporal locality. Based on the observation, HEAM stores all the R table embeddings inside the LUT that is located in each bg-PIM. R embeddings are directed to the LUT inside the bg-PIM as depicted in Figure 8 (b). As a result, the number of bank accesses in compositional embedding is reduced by half, making the total number of accesses equivalent to that of the original model. Additionally, given that the R embeddings follow a uniform distribution, load balance between LUT entries is achieved automatically. The total area overhead of LUT is minimal, as the number of entries required within the LUT is typically small considering the hash collision is usually set as a value less than 100. As we employ simple addition for input embedding reconstruction operation, we evenly allocate all the R tables across all LUTs in a random fashion without forcing the Q table and R table to be placed within the same bank group.

While bd-PIM could be considered for LUT placement, bg-PIM offers distinct advantages. Placing LUT within bd-PIM, which requires housing all R tables in the base die, leads to a substantial area overhead. The additional space needed for LUT placement on the base die is constrained by the presence of existing logic elements. This limitation becomes increasingly challenging as the number of tables, the frequency of hash collisions, and the sizes of the vectors grow. For instance, a model with 100 embedding tables, a hash collision of 50, and a vector size of 512B would require

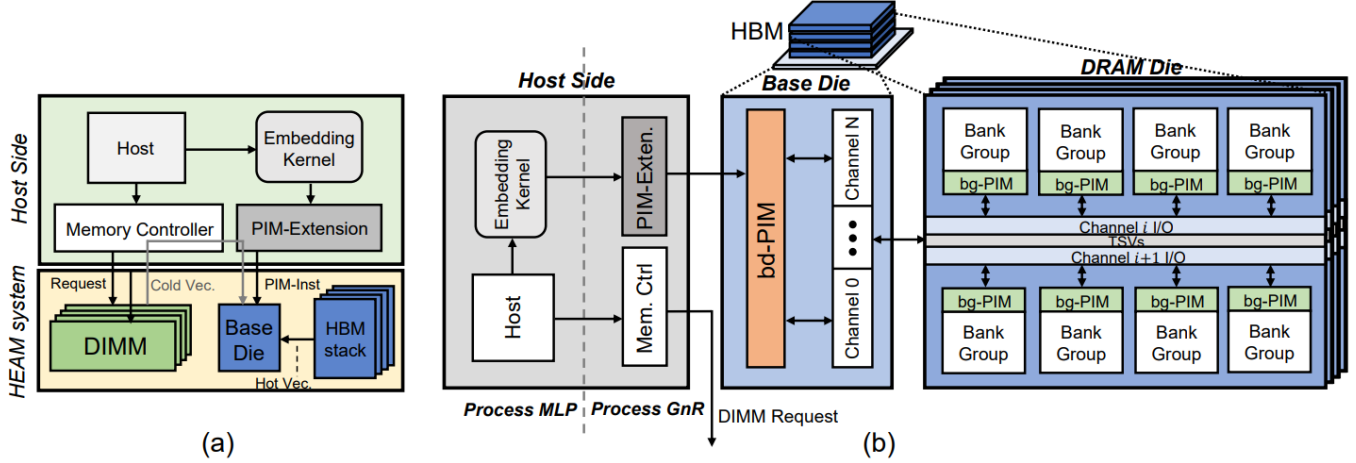


Figure 7. HEAM architecture. (a) Overview of HEAM architecture, (b) 2-level PIM system in HBM

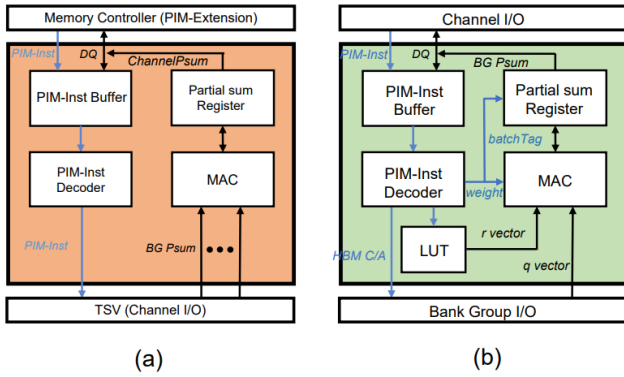


Figure 8. PIM architectures. (a) bd-PIM, (b) bg-PIM

an additional 2.44MB of area on the base die for the R table ($100 \text{ tables} \times 512\text{B} \times 50 \text{ collision}$). On the other hand, storing the R table in bg-PIM distributes these tables across the four dies of HBM. Each PIM in its respective bank group only requires an additional 80KB of area. Given that the typical bank group size in HBM is around 64MB, this area overhead is manageable. Moreover, this configuration can accommodate expansions in hash collision, total tables, and vector dimensions to a certain extent, making it a more scalable solution.

4.3 Hash Collision Value for HEAM System

As the Q table exhibits similar locality characteristics to the original, the advantage of heterogeneous memory systems described in SPACE [9] is applicable to compositional embedding. Moreover, to diminish the hash collision value, the HBM-only scenario incurs redundant bandwidth since it needs to introduce additional stacks to increase capacity, while the heterogeneous system achieves the same hash collision without extra bandwidth. In order to fully reap the

maximum bandwidth, each memory request ratio has to be equal to the bandwidth ratio, as displayed in the equation 1.

$$\frac{Request_{HBM}}{Request_{DIMM}} = \frac{BW_{HBM}}{BW_{DIMM}} \quad (1)$$

When HBM bandwidth is expanded with PIM, the overall HBM request should be enlarged to meet the above equation, forcing additional data offloading to the HBM. This might demand higher hash collision, leading to decreased model quality. However, long tail distribution compensates such problems as increasing cumulative requests of HBM requires a small amount of additional data. Therefore, there is no need to introduce extra hash collision to meet the bandwidth demand.

4.4 PIM Instructions and the Execution Flow

PIM Instructions. HEAM leverages the PIM instruction to deliver embedding operation information to each bg-PIM, following RecNMP [7] and TRiM [8]. The total width of a single PIM instruction is 84 bits. The *opcode* (3-bit) specifies the operation type that bd-PIM and bg-PIM should take into action for GnR operation. The *target address* (34-bit) denotes the start address of the PIM-Inst to read from the bank group. *nRD* (4-bit) indicates the vector size. The *weight* (32-bit) delivers weight information for weighted sum. *transfer* (1-bit) determines whether the partial sum is complete and ready to deliver. The *skewed-cycle* (6-bit) instructs bg-PIM the time that PIM instruction should be decoded after being delivered to the bg-PIM. The *batchTag* (2-bit) is the assigned batch of the PIM instruction.

Execution Flow. To run the PIM system, it is essential for the memory controller to deliver PIM instructions to the memory system properly. Like prior works [7], [8], [9], HEAM offers an embedding operation driver that extends

the current memory controller. The driver receives an embedding operation from the host, constructs PIM instructions, and offloads it to the NMP at the HBM. When HBM is used as a DRAM cache inside a heterogeneous memory system, a mapping of data is required to be stored inside the memory controller to direct each of the commands to the proper memory system. To support this, embeddings are mapped with a direct mapping method. With the aid of the direct mapping method, the memory controller could send PIM instructions and DDR4 commands to each memory by adopting the method used in SPACE [9]. To avoid the cache coherence issues, we allocate memory space dedicated to HEAM as uncachable. Additionally, to cope with the command/address (C/A) bandwidth overhead issue addressed before [8], we follow the method or prior works that utilize data (DQ) pins to deliver a number of instructions to bg-PIMs within a short cycle. Specifically, we utilize 14 C/A pins with 256-bit wide DQ pins to transfer 1 PIM instruction in a single cycle. Due to the abundant HBM DQ pins, HEAM successfully addresses the C/A bandwidth overhead.

5 Experimental Setup

Simulation Methodology. We modified DRAMsim3 [26], a cycle-accurate memory simulator, to implement and evaluate the performance of the HEAM system. HBM2 x128 and DDR4-3200 x8 were utilized as base memory systems for the HEAM system and the baselines. Table 2 summarizes the memory system configuration utilized in our experiment. Within a single DDR4-3200 x8 device, 2 ranks were employed. To utilize the heterogeneous memory systems, HEAM makes use of a flat addressable method, which has been continuously adopted in prior works on the same system configuration [9], [27], [28], [29]. We compare HEAM performance against previous NMP architectures, TensorDIMM [6], RecNMP [7], TRiM [8] and SPACE [9]. The traces of embedding operation were extracted from running the DLRM model, which is fed into the simulation framework.

In order to meet fair comparison, we treat all the embeddings within the R table as hot vectors so that temporal locality utilization techniques proposed in prior works could be maximally exploited. For instance, we mark every R table embedding with *localityBit* when implementing RecNMP. For TRiM implementation, R table embeddings have the highest priority when participating in *hot entry profiling*. In this case, vectors counted from the front of q vectors that are ordered with highest locality takes participation in hot entry profiling after R table. To fairly measure the performance of SPACE, *reduction locality* technique was employed, storing partial sums of hot vectors in the available space on HBM2.

Area and Power Consumption. To obtain the area and the power of PIM units, bd-PIM and bg-PIM were synthesized using Synopsys Design Compiler with 45nm CMOS technology operating at 300MHz clock frequency. For the

case of bg-PIM, the corresponding area was scaled to a 20nm DRAM processing. Area and the power of LUT used inside bg-PIM were estimated using CACTI [30].

Recommendation System Datasets. Obtaining a sufficiently large dataset is crucial for our experiment as HBM2 capacity needs to be fully occupied even after compositional embedding is applied regarding the assumption of the HEAM system. However, since datasets meeting such constraints is not publicly available, we utilize criteo datasets [24],[25] by setting its vector size large enough, 128B to 512B. Note that criteo-terabyte dataset [25] capacity is near 10 GB when the vector length is 64B.

Table 2. Memory System configurations

HBM2 x128 device	
Organizations	8 channels per 4-hi stack, 4 bank groups per channel
Timing parameters	tCL=14, tRP=14, tRCD=14, tCCD_S=1, tCCD_L=2, tBL=16
Clock frequency	1000MHz
DDR4-3200 x8 device	
Organizations	1 channel per DIMM, 2 ranks per channel, 4 bank groups per rank
Timing parameters	tCL=22, tRP=22, tRCD=22, tCCD_S=4, tCCD_L=8, tBL=8
Clock frequency	1600MHz

6 Evaluation Result

We evaluate the impact of HEAM’s design choices as the first step to analyze the effectiveness of each choice. We then compare the performance of HEAM with state-of-the-art NMP designs, which target the embedding operation. Additionally, hardware overhead introduced to the overall system for HEAM architecture support is analyzed. We assess the limitations of compositional embedding to explore the boundary in terms of compositional embedding could be applied to our system in terms of preserving model quality.

6.1 Performance Impact of Design Optimizations

Following TRiM [8], we demonstrate the impact of each design optimization choice on the speedup performance. Figure 9 displays the performance improvements when design optimizations are gradually incorporated in HEAM system. The baseline is the execution speed of HBM2 in conjunction with bd-PIM. The first scenario is *HEAM-BG*, where bg-PIM without LUT is located in each bank group. The following scheme is *CA compression*, when command address compression is applied to the HEAM-BG scenario. *Batching* corresponds to when the batching technique is applied to the HEAM system. Finally, *LUT* scheme adds LUT to Batching scenario, reducing direct access to the bank of R table. Applying all the optimization techniques achieves 2.8× higher result than

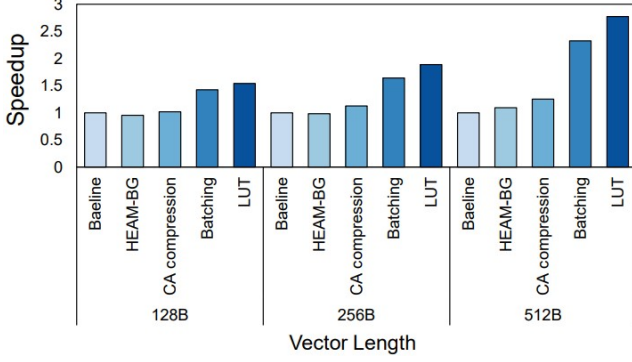


Figure 9. Performance Impact of Design Optimizations

the baseline when the vector size is 512B. HEAM-BG enhances the performance by 10% compared to the baseline. CA compression enhances 14% of the performance as the CA bandwidth overhead is mitigated by both utilizing the CA pin and DQ pin of HBM2. The batching scheme gains 86% of additional speedup by reducing load imbalance issues and satisfying the high demand of pooling size of bg-PIM utilized inside HBM2. The root of the performance benefit of Batching lies in pulling up the potential of bank group level parallelism. Finally, 19% more speedup is acquired in the LUT scenario, as it reduces the total DRAM access count by effectively utilizing the high temporal locality of the R table. Discussed highlights of each optimization technique increase as the vector length grows, leading to more frequent ACTs within each bank group, creating an environment that fully allows bg-PIM to capitalize its parallelism.

The primary reason for the relatively low speedup of HEAM-BG, even though it utilizes bg-PIM, is that the total embedding lookups in a single batch are small in the criterion dataset, resulting in low utilization of bg-PIM parallelism. The fact that baseline HBM2 is capable of embedding lookups of critero dataset due to its abundant channels further diminishes effect of HEAM-BG in this case. Coupled with the operation cycles of PIM and cycles required to deliver PIM instructions, this under-utilization issue especially worsens for small vector length. However, when batching is applied, total embedding lookups per operation increase, resulting in higher throughput than baseline.

6.2 Performance Evaluation with Previous NMP Designs

Speedup Comparison. To demonstrate the effectiveness of our proposal, we compare the overall performance of HEAM to the speedup in embedding operation of the previous works [6], [7], [8], [9]. In our experiment, a total of two DIMMs were utilized for previous DIMM-based NMP architectures.

Through the use of HBM, 2-level PIM structure, and off-loading techniques, HEAM achieved the best speedup across all the prior works. Figure 10 shows the relative performance

of configurations normalized to TensorDIMM, varying vector lengths from 128B to 512B. Compared to the prior works, HEAM achieves 6.3 \times , 4.6 \times , 2.3 \times , 1.8 \times speedup compared to TensorDIMM, RecNMP, TRiM-G, SPACE when vector length is 512B. Compared to SPACE, which also utilizes a heterogeneous memory system, HEAM’s superior achievement in speedup comes from the utilization of bg-PIM followed by design choices of batching and LUT. The performance enhancement of HEAM increases as vector length gets larger, as internal bandwidth becomes more utilized due to more frequent ACTs occurring inside the memory. A larger pooling size and larger vector length, a normal trend of recommendation systems in production, would result in even more enhancement.

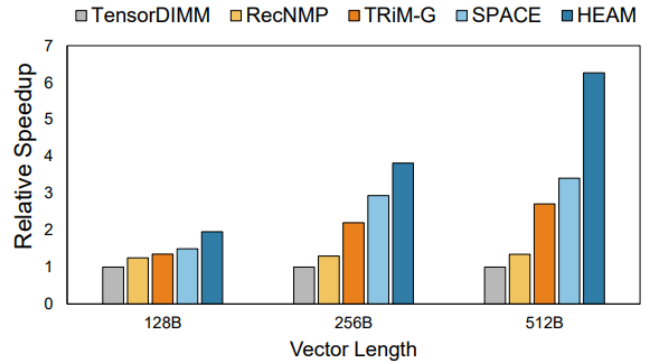


Figure 10. Performance evaluation on various NMP systems

Relative Energy Consumption. Figure 11 depicts the relative energy consumption of prior works and HEAM, which are normalized to the result of TensorDIMM. As shown in the figure, HEAM saves 58.9%, 45.9%, and 14.1% energy compared to TensorDIMM, RecNMP, and SPACE. HEAM saves 14.2% from SPACE energy consumption, similar to the amount of energy saved compared to TRiM-G.

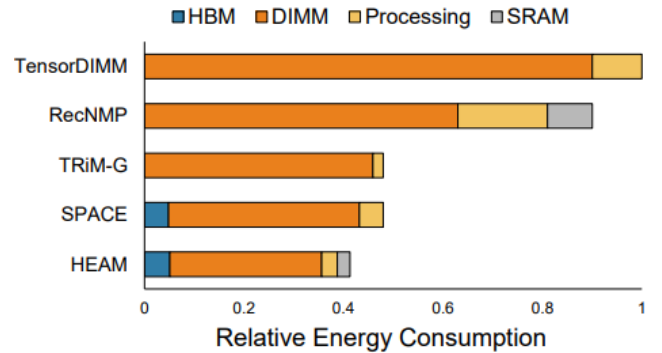


Figure 11. Relative energy consumption in NMP models

6.3 Design Overhead

The total area occupied by bg-PIM is 3.12mm^2 per HBM2 die, which takes a 3.44% portion of each HBM2 die. LUT consists of 20KB SRAM which takes 10% of the total PIM area. Each PIM includes four MAC units, register files for buffer and logic support. The total gate count is 118,087 per each bg-PIM. The energy consumption of LUT accounts for 0.04% of total energy consumed by HEAM, which enables high energy savings from DRAM access.

6.4 Assessment of Compositional Embedding Shortcomings

Efficiency of Increasing Hash Collision. To achieve the necessary bandwidth ratio between HBM and DIMM, reducing the total number of hot vectors should coincide with an increase in hash collisions, especially since the total hot vectors might surpass the capacity of a single HBM stack in production scenarios. Ideally, hot vectors would be grouped closely, allowing a quotient hash function to map consecutive hot vectors to the same Q vector. This would inversely reduce the total number of hot vectors relative to the increase in hash collisions. However, this ideal situation is rare. In the worst-case scenario, the reduction in total hot vectors is minimal, as cold vectors typically outnumber and surround each hot Q vector, leading to only a marginal decrease.

To verify the reduction efficiency, we measured the changes in the number of the hot vectors while modifying hash collision value on public datasets available online [24], [31]. In this experiment, we defined hot vectors as the vectors needed to achieve 80% of the cumulative request. The result is shown in Figure 12 (a). Although the result indicates the hot vectors are not clustered ideally, increasing hash collision still decreases hot vectors, which is enough to meet the bandwidth ratio demand between HBM and DIMM.

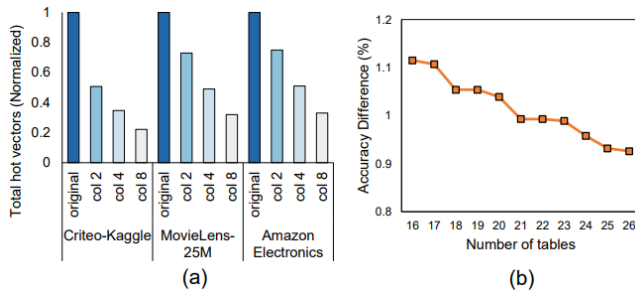


Figure 12. Compositional embedding shortcoming analysis. (a) Change in the number of hot vectors based on the hash collision value across criteo-kaggle, movielens-25M, amazon electronics. (b) Accuracy difference between the original model and the model trained with compositional embedding by hash collision 4.

Decrease in model quality drop with more embedding tables. As more embedding tables are used in the recommendation system, the model quality increases [5]. At the production level, it is known that there are 10s of embedding tables. As the accuracy drop of compositional embedding is due to the mixture of distinctive embeddings [21], applying more embedding tables might resolve the accuracy drop caused when applying the algorithm. To see the effect of embedding tables on the accuracy, we conducted experiments in criteo-kaggle-dataset. Since some tables are used more often than others, we picked randomly the tables to be excluded, averaging the result of 3 experiments. The overall result is shown in Figure 12 (b). By excluding tables from 10 to 0, we found that the gap of accuracy drop decreases.

7 Conclusions

We introduce HEAM, a 3-level PIM architecture that comprises DIMM, HBM featuring bd-PIM and bg-PIM with LUT. Our goal is to accelerate compositional embedding. We have examined the distinct traits of compositional embedding and leveraged our findings to boost overall throughput. Our system tackles two key challenges in DLRM: model size expansion and memory-bound operations. In addition, HEAM effectively resolves the issue of double memory access that arises when applying compositional embedding, resulting in $6.3\times$ performance improvement and 58.9% energy savings compared to the previous NMP architectures tailored for recommendation systems.

References

- [1] Maxim Naumov, Dheevatsa Mudigere, Hao-Jun Michael Shi, Jianyu Huang, Narayanan Sundaraman, Jongsoo Park, Xiaodong Wang, Udit Gupta, Carole-Jean Wu, Alisson G Azzolini, et al. Deep learning recommendation model for personalization and recommendation systems. *arXiv preprint arXiv:1906.00091*, 2019.
- [2] Paul Covington, Jay Adams, and Emre Sargin. Deep neural networks for youtube recommendations. In *Proceedings of the 10th ACM conference on recommender systems*, pages 191–198, 2016.
- [3] Harald Steck, Linas Baltrunas, Ehtsham Elahi, Dawen Liang, Yves Raimond, and Justin Basilico. Deep learning for recommender systems: A netflix case study. *AI Magazine*, 42(3):7–18, 2021.
- [4] Udit Gupta, Carole-Jean Wu, Xiaodong Wang, Maxim Naumov, Brandon Reagen, David Brooks, Bradford Cottel, Kim Hazelwood, Mark Hempstead, Bill Jia, et al. The architectural implications of facebook’s dnn-based personalized recommendation. In *2020 IEEE International Symposium on High Performance Computer Architecture (HPCA)*, pages 488–501. IEEE, 2020.
- [5] Mark Zhao, Niket Agarwal, Aarti Basant, Buğra Gedik, Satadru Pan, Mustafa Ozdal, Rakesh Komuravelli, Jerry Pan, Tianshu Bao, Haowei Lu, et al. Understanding data storage and ingestion for large-scale deep recommendation model training: Industrial product. In *Proceedings of the 49th Annual International Symposium on Computer Architecture*, pages 1042–1057, 2022.
- [6] Youngeun Kwon, Yunjae Lee, and Minsoo Rhu. Tensordimm: A practical near-memory processing architecture for embeddings and tensor operations in deep learning. In *Proceedings of the 52nd Annual IEEE/ACM International Symposium on Microarchitecture*, pages 740–753, 2019.

- [7] Liu Ke, Udit Gupta, Benjamin Youngjae Cho, David Brooks, Vikas Chandra, Utku Diril, Amin Firoozshahian, Kim Hazelwood, Bill Jia, Hsien-Hsin S Lee, et al. Recnmp: Accelerating personalized recommendation with near-memory processing. In *2020 ACM/IEEE 47th Annual International Symposium on Computer Architecture (ISCA)*, pages 790–803. IEEE, 2020.
- [8] Jaehyun Park, Byeongho Kim, Sungmin Yun, Eojin Lee, Minsoo Rhu, and Jung Ho Ahn. Trim: Enhancing processor-memory interfaces with scalable tensor reduction in memory. In *MICRO-54: 54th Annual IEEE/ACM International Symposium on Microarchitecture*, pages 268–281, 2021.
- [9] Hongju Kal, Seokmin Lee, Gun Ko, and Won Woo Ro. Space: locality-aware processing in heterogeneous memory for personalized recommendations. In *2021 ACM/IEEE 48th Annual International Symposium on Computer Architecture (ISCA)*, pages 679–691. IEEE, 2021.
- [10] Liu Ke, Xuan Zhang, Jinin So, Jong-Geon Lee, Shin-Haeng Kang, Sukhan Lee, Songyi Han, YeonGon Cho, Jin Hyun Kim, Yongsuk Kwon, et al. Near-memory processing in action: Accelerating personalized recommendation with axdim. *IEEE Micro*, 42(1):116–127, 2021.
- [11] Bahar Asgari, Ramyad Hadidi, Jiashen Cao, Sung-Kyu Lim, Hyesoon Kim, et al. Fafnir: Accelerating sparse gathering by using efficient near-memory intelligent reduction. In *2021 IEEE International Symposium on High-Performance Computer Architecture (HPCA)*, pages 908–920. IEEE, 2021.
- [12] Geet Sethi, Bilge Acun, Niket Agarwal, Christos Kozyrakis, Caroline Trippel, and Carole-Jean Wu. Recsharp: statistical feature-based memory optimization for industry-scale neural recommendation. In *Proceedings of the 27th ACM International Conference on Architectural Support for Programming Languages and Operating Systems*, pages 344–358, 2022.
- [13] Dheevatsa Mudigere, Yuchen Hao, Jianyu Huang, Zhihao Jia, Andrew Tulloch, Srinivas Sridharan, Xing Liu, Mustafa Ozdal, Jade Nie, Jongsoo Park, et al. Software-hardware co-design for fast and scalable training of deep learning recommendation models. In *Proceedings of the 49th Annual International Symposium on Computer Architecture*, pages 993–1011, 2022.
- [14] Ehsan K Ardestani, Changkyu Kim, Seung Jae Lee, Luoshang Pan, Jens Axboe, Valmiki Rampersad, Banit Agrawal, Fuxun Yu, Ansha Yu, Trung Le, et al. Supporting massive dlm inference through software defined memory. In *2022 IEEE 42nd International Conference on Distributed Computing Systems (ICDCS)*, pages 302–312. IEEE, 2022.
- [15] Liu Ke, Udit Gupta, Mark Hempstead, Carole-Jean Wu, Hsien-Hsin S Lee, and Xuan Zhang. Hercules: Heterogeneity-aware inference serving for at-scale personalized recommendation. In *2022 IEEE International Symposium on High-Performance Computer Architecture (HPCA)*, pages 141–154. IEEE, 2022.
- [16] Amin Firoozshahian, Joel Coburn, Roman Levenstein, Rakesh Nattoji, Ashwin Kamath, Olivia Wu, Gurdeepak Grewal, Harish Aepala, Bhasker Jakka, Bob Dreyer, et al. Mtia: First generation silicon targeting meta’s recommendation systems. In *Proceedings of the 50th Annual International Symposium on Computer Architecture*, pages 1–13, 2023.
- [17] Weijie Zhao, Jingyuan Zhang, Deping Xie, Yulei Qian, Ronglai Jia, and Ping Li. Aibox: Ctr prediction model training on a single node. In *Proceedings of the 28th ACM International Conference on Information and Knowledge Management*, pages 319–328, 2019.
- [18] Hao-Jun Michael Shi, Dheevatsa Mudigere, Maxim Naumov, and Jiyan Yang. Compositional embeddings using complementary partitions for memory-efficient recommendation systems. In *Proceedings of the 26th ACM SIGKDD International Conference on Knowledge Discovery & Data Mining*, pages 165–175, 2020.
- [19] Antonio A Ginart, Maxim Naumov, Dheevatsa Mudigere, Jiyan Yang, and James Zou. Mixed dimension embeddings with application to memory-efficient recommendation systems. In *2021 IEEE International Symposium on Information Theory (ISIT)*, pages 2786–2791. IEEE, 2021.
- [20] Chunxing Yin, Bilge Acun, Carole-Jean Wu, and Xing Liu. Tt-rec: Tensor train compression for deep learning recommendation models. *Proceedings of Machine Learning and Systems*, 3:448–462, 2021.
- [21] Fuyuan Lyu, Xing Tang, Hong Zhu, Huifeng Guo, Yingxue Zhang, Ruiming Tang, and Xue Liu. Optembed: Learning optimal embedding table for click-through rate prediction. In *Proceedings of the 31st ACM International Conference on Information & Knowledge Management*, pages 1399–1409, 2022.
- [22] Kilian Weinberger, Anirban Dasgupta, John Langford, Alex Smola, and Josh Attenberg. Feature hashing for large scale multitask learning. In *Proceedings of the 26th annual international conference on machine learning*, pages 1113–1120, 2009.
- [23] Wang-Cheng Kang, Derek Zhiyuan Cheng, Tiansheng Yao, Xinyang Yi, Ting Chen, Lichan Hong, and Ed H Chi. Learning to embed categorical features without embedding tables for recommendation. In *Proceedings of the 27th ACM SIGKDD Conference on Knowledge Discovery & Data Mining*, pages 840–850, 2021.
- [24] CriteoLabs. 2014. Kaggle display advertising challenge dataset. <https://jmcauley.ucsd.edu/data/amazon/>.
- [25] Vijay Janapa Reddi, Christine Cheng, David Kanter, Peter Mattson, Guenther Schmuelling, Carole-Jean Wu, Brian Anderson, Maximilien Breughe, Mark Charlebois, William Chou, et al. Mlperf inference benchmark. In *2020 ACM/IEEE 47th Annual International Symposium on Computer Architecture (ISCA)*, pages 446–459. IEEE, 2020.
- [26] Shang Li, Zhiyuan Yang, Dhiraj Reddy, Ankur Srivastava, and Bruce Jacob. Dramsim3: A cycle-accurate, thermal-capable dram simulator. *IEEE Computer Architecture Letters*, 19(2):106–109, 2020.
- [27] Jaewoong Sim, Alaa R Alameldeen, Zeshan Chishti, Chris Wilkerson, and Hyesoon Kim. Transparent hardware management of stacked dram as part of memory. In *2014 47th Annual IEEE/ACM International Symposium on Microarchitecture*, pages 13–24. IEEE, 2014.
- [28] Chia Chen Chou, Aamer Jaleel, and Moinuddin K Qureshi. Cameo: A two-level memory organization with capacity of main memory and flexibility of hardware-managed cache. In *2014 47th Annual IEEE/ACM International Symposium on Microarchitecture*, pages 1–12. IEEE, 2014.
- [29] Chiachen Chou, Aamer Jaleel, and Moinuddin K Qureshi. Bear: Techniques for mitigating bandwidth bloat in gigascale dram caches. *ACM SIGARCH Computer Architecture News*, 43(3S):198–210, 2015.
- [30] Naveen Muralimanohar, Rajeev Balasubramanian, and Norman P Jouppi. Cacti 6.0: A tool to model large caches. *HP laboratories*, 27:28, 2009.
- [31] movielens. 2019. Movielens 25m dataset. <https://grouplens.org/datasets/movielens/25m/>.